Probabilistic kinematic model of a robotic catheter for 3D position control

Bingbin Yu[1], José de Gea Fernández[1], Tao Tan[2]

Abstract

Continuum robots offer compliant and dexterous operations, which are suitable to be used in unstructured environments. Tendon-driven catheters, owing to their continuum structure, are applied in minimal invasive surgeries such as intracardiac interventions. However, due to the intrinsic nonlinearities and external disturbances, it is still a challenging task to accurately steer the catheter tip to the desired 3D positions. In this paper, we proposed a new probabilistic kinematic model and a model-based three-dimensional position control scheme for a tendon-driven cardiac catheter. A dynamic Gaussian-based probabilistic model is developed to learn a mapping from the catheter states to the control actions. Based on the probabilistic model, a closed-loop position control is developed, in which the catheter is driven by a new designed catheter driver system and tracked by a multiple near-infrared cameras system. The proposed catheter framework is evaluated by the 3D trajectory tracking experiments both in a real 3D open space and in a minimum-energy based simulator. The proposed control framework approximates the general kinematic by a combination of a catheter translation model and a distal workspace model, which provide the ability of automatically positioning the catheter tip in 3D and improving the accuracy by compensating the learned nonlinear effects.

Keywords: robotic catheter, probabilistic model, optical tracking, position control, surgical robot

1. Introduction

A cardiac catheter is a continuum steerable tube which is used in cardiac cauterization, an effective minimal invasive cardiac treatment. Conventionally, the catheter is operated by surgeons and monitored from fluoroscopic images. Due to the complexity of the environment, it is difficult to accurately position the catheter's tip even for an experienced surgeon. Moreover, the long time and frequent operations increases the radiation risk for the surgeons.

Currently, there are several commercial robotic catheter systems available to assist the cardiac cauterization procedure, e.g. Sensei (Hansen Medical,Inc), Amigo (Catheter robotics,Inc) and CorPath (Corindus,Inc). All these systems provide a tele-operation workstation that allow the operators to remotely navigate and control the catheters. Nonetheless, the remote manual catheter control still requires significant surgical skills. For achieving accurate and automatic catheter tip positioning, a precise model is required which has been investigated by a number of research groups that are either focusing on the cardiac catheters or in a more general context of continuum robot.

Continuum robots do not contain rigid links, instead the structures bend continuously and smoothly along their length in their steerable section. Due to the non-linear property of elastomeric materials and the characteristics of the actuation system, precise kinematic modelling of the continuum robot is still a challenging task. In the past several years, various static and dynamic kinematic models were developed, a considerable part of which are based on the Piecewise Constant Curvature (PCC) assumption. This method assumes that the continuum robot is composed by multiple constant curvature sections and, as a result, its model can be ultimately decomposed into a robot specific and a robot independent mapping, which, for instance, is surveyed in great detail in [1] [2]. Although the PCC assumption is widely used, it often oversimplifies the internal dynamics and external disturbances, and thus it might introduce inaccuracies into the later kinematic control.

Besides the PCC assumption, other model-based approaches have also been developed to address the real dynamic effects, aiming at modelling the non-constant curvature of continuum robots. The Cosserat rod method[3][4] describes a kinematic model very precisely, but there is no close-form solution for a tendon-driven catheter yet since the initial boundary values of its nonlinear differential equation need to be solved numerically. Kang et al.[5] uses a spring-mass method, which divides a continuum arm into multiple segments. Each segment consists of longitudinal 'muscles' and other components considered as a mass-spring-damper system. However, this model becomes computationally-expensive when robot length increases.

Comparing to the other continuum robots which usually are mounted on a fixed base, a cardiac catheter needs

[1]Robotics Innovation Center at German Research Center for Artificial Intelligence (DFKI), Robert-Hooke Str. 1, 28359 Bremen, Germany

[2]Department of Biomedical Engineering, Eindhoven University of Technology, 5600 MB Eindhoven , The Netherlands

to be inserted through the aorta to the heart chambers plus the catheter tip is required to locate 3D target positions. As a result, the translational movement should be included in the kinematic model as well. However, due to the catheter intrinsic nonlinearity, compliant construction and even the interaction of the catheter with the environment, there are very few groups which investigate the catheter 3D positioning. Loschak et al.[6] proposed a control approach which enables autonomously positioning of a Intracardiac echocardiography (ICE) catheter in a 3D open space. However, the approach applied a classic kinematic model based on several assumptions which neglect the intrinsic nonlinearities and compliances. Since the cardiac catheter usually is only steerable in the distal section, it also has been considered as a semi-rigid link: Back et al.[7] proposes a model-free control approach which enables the catheter tip to follow a target circle with a selected 3 mm error margin. Tran et al.[8] uses a minimum energy model to estimate appropriate steering actions to move the catheter tip to a desired pose. Whilst the catheter is modelled by using Finite Element Method (FEM), which is a computationally consuming approach, the proposed real-time position control is validated in a 2D aorta phantom. The above mentioned methods have not modelled the external disturbances yet, such as gravity and external interaction, which are recently considered in machine learning approaches.

Neural networks (NNs) were initially used in continuum robot control by Braganza et al.[9] to compensate the uncertain non-linear errors and recently used to model the kinematics by Giorelli et al.[10] and Runge et al. [11]. The probabilistic based approaches are also used in inverse kinematics modelling and control by Xu et al.[12], Lee et al.[13]. But these approaches focus on continuum robots either mounted on a fixed base or in which the linear motion (translation) is not taken into account, as in [12].

In this paper, we investigate a probabilistic approach to model the catheter steering including the translational movement. Based on the model, we further proposed a catheter tip position control framework. The rest of the paper is organized as follows: In Section 2, the dynamic Gaussian mixture model-based modelling approach is presented, Section 3 describes a novel catheter driver hardware design and an optical tracking system that is used to perceive the catheter shape. In Section 4, the data-based catheter kinematics and the position control scheme are proposed and the control performance is evaluated in a real experimental setup. Finally, the paper is concluded in Section 5.

2. Modelling Method

2.1. Introduction to Dynamic Gaussian Mixture Model (DGMM)

A Gaussian Mixture Model (GMM) is a parametric probability density function represented as a weighted sum of Gaussian component densities, which are widely used in modeling complex and multi-variable data [14]. In case of the catheter modelling problem, a dynamic Gaussian mixture model (DGMM) is used to represent the catheter kinematic model, in which the number of Gaussian components can vary to enable the model to optimally fit the system.

The DGMM represents a probability density function $P(x)$ as a variable-sized set of weighted Gaussian pairs (Eq. 1).

$$p(x) = \sum_{i=1}^{m} \hat{\omega_i} g(x|\mu_i, \Sigma_i), \tag{1}$$

where $g(x|\mu_i, \Sigma_i)$ are the component Gaussian densities, m is the number of Gaussian components which is varying in the training phase and each Gaussian function is represented by

$$g(x|\mu_i, \Sigma_i) = \frac{1}{(2\pi)^{\frac{N}{2}} |\Sigma_i|^{\frac{1}{2}}} exp - \frac{1}{2}(x-\mu_i)^T \Sigma_i^{-1}(x-\mu_i), \tag{2}$$

with mean vector μ_i and covariance matrix Σ_i. $\hat{\omega_i}$ is the weight of each component Gaussian

$$\hat{\omega_i} = \omega_i / \Sigma_{k=1}^{m}. \tag{3}$$

The quantity x is the observation vector. In case of catheter kinematic model, the vector x is made up of vectors $[\vec{S_{t+1}}, \vec{S_t}, \delta_l, \delta_d]$, where $\vec{S_t}$ and $\vec{S_{t+1}}$ indicate the current catheter state and next state after actions, δ_l is the insert action provided from the linear driver and δ_d represent the displacement of the catheter handle which pulled by the pitch driver (see Fig. 6). As a result, the catheter kinematic model is represented by the joint probability density function:

$$P[\vec{S_{t+1}}, \vec{S_t}, \delta_l, \delta_d]. \tag{4}$$

In order to characterize the catheter current state, $\vec{S_t}$ is given by

$$\vec{S_t} = \begin{bmatrix} \alpha_t \\ \phi_t \\ r_t \\ d_t \end{bmatrix} \tag{5}$$

As Figure 1 shows, α_t is the current catheter shape which is represented by the parameters of a fitted B-spline, ϕ_t is the pitch angle of the catheter distal section, r_t is the rotation angle from initial angle and d_t is the pulled displacement of the catheter handle.

Expanding Eq.4 with Eq.5, the catheter kinematic model can be written as:

$$P[\alpha_{t+1}, \phi_{t+1}, r_{t+1}, d_{t+1}, \alpha_t, \phi_t, r_t, d_t, \delta_l, \delta_d]. \tag{6}$$

2.2. Online update method

In this section, we describe the method used for updating the DGMM kinematic model by the sensory data.

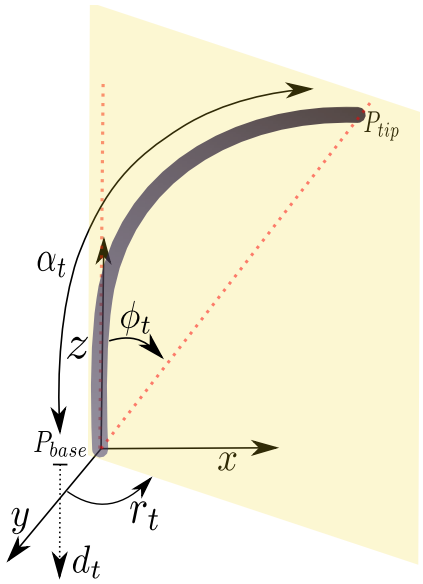

Figure 1: An illustration of the coordinate frame of the catheter distal section and the features used to characterize the catheter current state.

Since the catheter is tracked by a multiple near-infrared camera system at high frequency (500Hz), it is necessary to assess each new observation data before it assimilated into the existing model. Therefore, an online update approach is used which is depicted in Algorithm 1.

Data: a single observation vector $\vec{x}$.
Result: online update the catheter kinematic model with each new observation vector.
Function: $DGMM\_Online\_Kmeans(x, \delta^2, L_r, N_k)$:
initial covariance magnitude δ^2;
learning rate L_r;
number of kmeans cluster N_k;
if $number\_of\_x < N_k$ **then**
  add $\vec{x}$ into DGMM as a new gaussian;
else
  select the gaussian G_i from DGMM with a minimum RMSE to $\vec{x}$;
  update a new mean of the gaussian G_i with $\vec{x}$
  $mean(G_i)_{new} = mean(G_i) + L_r * (mean(G_i) - \vec{x})$.
end

Algorithm 1: Catheter kinematic model update.

2.3. Regression equation for DGMM estimation

For estimating the next state of the catheter, the expectation $E[\vec{S_{t+1}}|\vec{S_t}, \delta_l, \delta_d]$ needs to be calculated. For a mixture of Gaussians G and, for the sake of generality, let the mean of a Gaussian g_i be given by:

$$\mu_i = [\mu_i^{S_{t1}}, \mu_i^{S_t}, \mu_i^l, \mu_i^d], \tag{7}$$

and covariance by

$$\Sigma_i = \begin{bmatrix} \Sigma_i^{S_{t1}S_{t1}} & \Sigma_i^{S_{t1}S_t} & \Sigma_i^{S_{t1}l} & \Sigma_i^{S_{t1}d} \\ \Sigma_i^{S_tS_{t1}} & \Sigma_i^{S_tS_t} & \Sigma_i^{S_tl} & \Sigma_i^{S_td} \\ \Sigma_i^{lS_{t1}} & \Sigma_i^{lS_t} & \Sigma_i^{ll} & \Sigma_i^{ld} \\ \Sigma_i^{dS_{t1}} & \Sigma_i^{dS_t} & \Sigma_i^{dl} & \Sigma_i^{dd} \end{bmatrix} \tag{8}$$

The conditional mean for Gaussian g_i is a linear function given by

$$m_i(z) = E_i[Y|Z = z] = \mu_i^Z + \Sigma_i^{YZ}(\Sigma_i^{ZZ})^{-1}(z - \mu_i^Z), \tag{9}$$

and the conditional variance is given by

$$\delta_i^2 = Var_i[Y|Z = z] = \Sigma_i^{YY} - \Sigma_i^{YZ}(\Sigma_i^{ZZ})^{-1}\Sigma_i^{ZY}. \tag{10}$$

Now the conditional mean of $E[Y|Z = z]$ can be calculated by using

$$E[Y|Z = z] = \sum_{i=1}^{m}(\pi_i(z)m_i(z)), \tag{11}$$

where

$$\pi_i(z) = \frac{\omega_i\mathcal{N}(z; \mu_i, \Sigma_i)}{\Sigma_{k=1}^m \omega_k\mathcal{N}(z; \mu_k, \Sigma_k)} \tag{12}$$

3. Hardware design and experimental setup

3.1. A novel catheter driver system

A catheter driver system is developed in this study (Fig.2), which is composed by a linear stage (PI linear stage M-403.8DG; travel range: 200 mm, resolution: 0.018 μm), a pitch driver (0.5 mm/step in catheter handle), a roll driver (range: 360 degree, resolution: 0.0349 rad), a micro-controller (Arduino Nano V3.0 with an ATMEGA 328P). In order to grip the catheter and protect it during operation, a "Kellems Grip"[15] is used, which evenly distributes the grip force on the catheter body by using a flexible textile sleeve.

3.2. Optical tracking of an ablation catheter

A commercial tendon-driven ablation catheter from EndoSense SA is used which consists of a plastic handle that can be operated in translation and rotation. The catheter distal section (see Fig.3) is driven by a pull wire that connects the catheter handle to a point at the distal tip. Through the translational operation of the handle, the catheter distal section can be steered in a one-bending direction.

In order to perceive the catheter shape, five Qualisys Oqus-300 near-infrared cameras are used and mounted around the test-bed at 1.5 meters from the catheter and six passive reflective tapes (2.45 mm) are attached equally on the catheter body from distal tip to distal bend point with a distance 13 mm to each other. The Qualisys Oqus-300 provides 1.3 mega-pixels and 500 fps speed, which is able to measure a dynamic passive marker in sub-millimetre accuracy and static passive marker with a noise level less

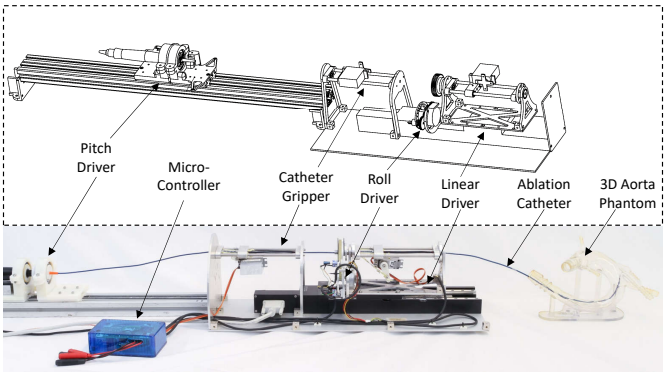

Figure 2: Catheter driver system, upper: Design of the catheter driver which is composed by a linear driver, a pitch driver, roll driver and a catheter gripper; lower: photo of the catheter driver with a tendon-driven ablation catheter and a 3D printed aorta phantom.

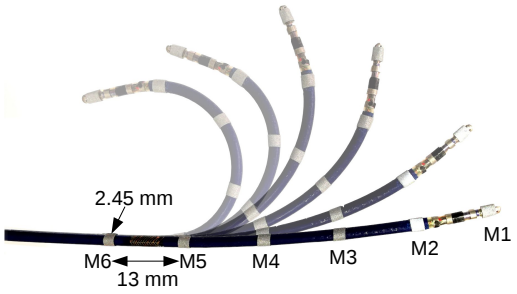

Figure 3: Distal section of a tendon-driven ablation catheter, 6 reflective markers are attached on the catheter body with equal distance (approximately 13 mm) to each other.

than 0.05 mm [16]. To evaluate our optical tacking for the attached markers, a single marker based test is conducted, which measures a 2 mm diameter static marker in 5 minutes with a sampling frequency of 185 Hz. The mean distance error and standard deviation reaches a precision of 0.0242±0.0159 mm.

The improvement in resolution compared to electromagnetic tracking system is significant. For instance, the Aurora 6-Dof EM sensor theoretically can provide a position measurement with a precision of about 0.48-0.8 mm and 0.3 degree within the field generator's working volume [17], with which it is challenging to measure a catheter tip aimed to be controlled with a position error of less than 2 mm. Comparing to conventional stereo cameras (e.g. clinical-used optical tracking system NDI polaris), a setup with multiple NIR cameras solves the problem of self-occlusion and the long wavelength enhances its tracking stability against the light refraction of the plastic organ phantom. As a result, it is one of the optimal solutions for tracking a soft surgical tools in open space or a plastic phantom having as a purpose the validation of a research application.

4. Catheter kinematics and control

4.1. Strategy of forward kinematics

Roll of distal section. As introduced in Section 2, the model of the catheter is represented by a joint probability density function: Eq.6, which is composed by catheter current state, next state and the corresponding actions: δ_l, δ_d. In this paper, the rotation of the catheter handle (roll of distal section) is assumed to be a rigid action, the rotational elasticity due to the catheter body is simplified. Therefore the roll of catheter distal section is represented by $r_{des} = r_t + \delta_r$ where r_{des} is the desired roll angle and δ_r is the roll action of the handle.

Pitch of distal section. Regarding the pitch of tendon driven catheters, due to the internal friction and backlash, the hysteresis effects are found and investigated by many research groups e.g.[18],[19] as well as in our previous investigation [20]. The forward kinematic of catheter pitch derived from the learned DGMM model Eq.6 and the regression Eq.9, which is represented by:

$$E[\alpha_{des}, \phi_{des} | \vec{S}_t, \delta_d] \tag{13}$$

where α_{des} is the desired catheter shape and the pitch angle ϕ_{des} can be calculated from the distal shape. The pitch model can be also trained independently by repeating the pitch experiments that increase and decrease the distal pitch angle and the observation vector $[\alpha_{t+1}, \phi_{t+1}, d_{t+1}, \alpha_t, \phi_t, d_t, \delta_d]$ is updated to a DGMM model P_{pitch}. After training, the catheter shape can be estimated with given current state α_t, ϕ_t, d_t and action δ_d.

In order to evaluate the forward kinematic model of catheter distal pitch, the distal section is steered to a fully-bent state, then to fully-released state by the pitch driver in six repeated experiments. Given pitch command δ_d in 1 step per action from pitch driver and last state S_{t-1}, the current position of the 6 passive markers is estimated by $E[P_{m_{1\sim6}} | S_{t-1}, \delta_d]$ as illustrated in Fig.4.

As can be seen from the Figure, the red dots are the measured markers from the optical sensors and blue diamonds are the predicted markers from a trained pitch model P_{pitch}. In this plot, the predicted markers after each action and corresponding trajectories in the test match the measured results closely. The mean Euclidean distances and standard deviation between the measured markers and the predicted markers in the repeated experiments are calculated and shown in Fig.5, where M_1 represents the catheter tip and M_6 is the base point. As it can be seen, the tip point presents the largest pitch movements and a small displacement can be found between the trajectories of bending and stretching. Since the catheter tip $M1$ presents the largest movement in each step and catheter point $M6$ keeps almost static during the experiments, the closer the markers are attached to the catheter tip, the larger the prediction deviation. As shown in Fig.3, a bend-deadzone is found in the Endosense ablation catheter, by

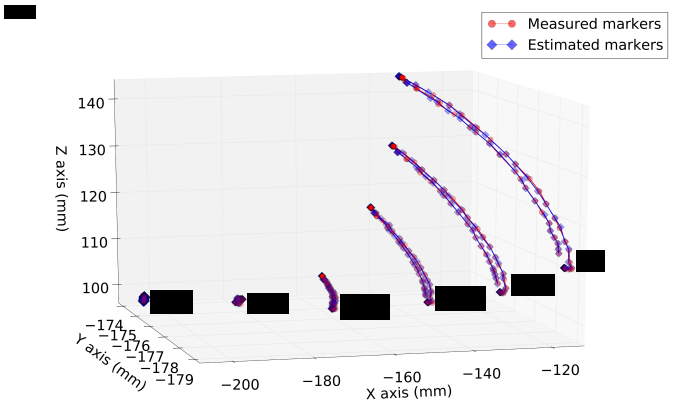

Figure 4: Prediction of the catheter distal shape by using a dynamic Gaussian mixture model with measured current shape and a pitch action.

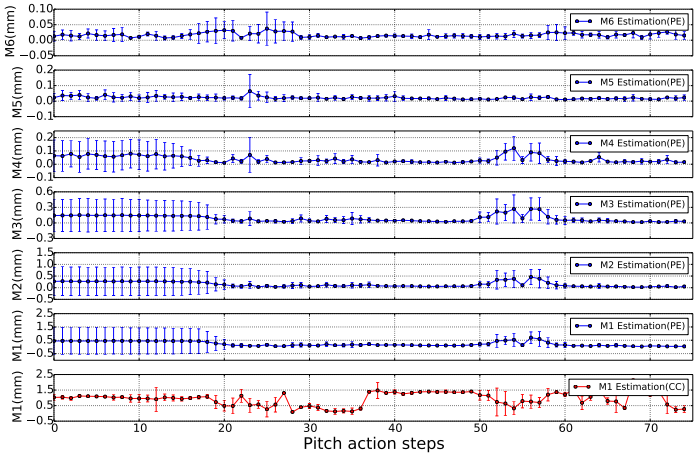

Figure 5: Mean distances and standard deviation of the markers estimation by using a trained DGMM distal model and a constant curvature method.

which the catheter distal section cannot be fully stretched to zero degree due to the internal friction. As a result, the small-scale displacements can be found in the initial states among the repeated experiments, which causes the standard deviations to be larger than the other pitch actions. It is noticeable that the prediction errors are large in between pitch actions 52 to 58, which corresponds to the bend procedure that starts to stretch from fully-bent state. Due to the hysteresis effects of the tendon system that can not be perfectly modelled, the error of this section is relatively large. From plot $M6$, the catheter base point presents an excellent estimation performance. Since it keeps almost static during the experiments, this error is mainly derived from the optical tracking system, which is slightly larger than its noise-level.

The curvature is described by radius R and circle center point P, that are calculated by using markers $M3, M4$ and $M5$. The length between the marker $M1$ and $M3$ is approximately 16mm and the catheter distal section is assumed on the same plane. As a result, the position of the marker $M1$ can be calculated. The mean Euclidean distances and standard deviation between the calculated $M1$ and measured tip point in the same repeated experiments are calculated and plotted in the last subplot of Fig.5. As the figure shows, the mean distance error of the constant curvature (CC) method is larger than the probabilistic estimation (PE). Since the $M1$ in constant curvature method is calculated from the measured points $M3, M4$ and $M5$, it presents a lower standard deviation at the beginning of each experiment.

Comparison with other modelling methods. As previously introduced, there are various methods for modelling steerable catheters, which trade-off model accuracy and computational expense. Considering the model accuracy, high-fidelity approaches such as Cosserat rod method [3][4] and minimum-energy approaches [8][21] would be candidates to be compared with the probabilistic model presented in this work. To the authors' knowledge, the closest works in position control are the one using a minimum-energy approach [8], which requires of very expensive numerical computation for a real-time position control and the Cosserat rod method used in [4], which requires knowledge of forces acting on the robot and relies on the target (tissue) motion, information which is not obtainable in the work presented here. On the other side, the popular piecewise constant curvature method [1][2] can be decomposed into a robot-specific and a robot-independent mappings. The robot-specific mapping transforms actuator actions to configuration space variables (arc curvature, tendon length, etc) and the robot-independent mapping brings the configuration space variables into task space. The methods for robot-specific mapping are reviewed in section 3.2 of the work in [1] and require of precise information of the tendon lengths and the arc curvature k (which is obtained by geometric analysis of multiple tendons). Since the steerable catheter used in this work is a commercial single-tendon product, from which the length of the internal tendon is difficult to be precisely measured, the conventional geometric analysis using the arc parameter k cannot be analyzed for our system. For that reason, recent research works in position control of single tendon catheter using the constant curvature assumption ([6][22]) are approximating the catheter distal shaft by a circle shape. The work in [22] compensates the backlash effects by using a experimentally-based method, which presents a better performance than the ideal constant curvature. However, despite the internal compensation of nonlinearities, the curvatures along the distal shaft are still different, which brings deviation in estimating the distal shape.

As can be seen from the last two subplots of Figure 5, the result of our probabilistic model is estimated by using the applied actions from the catheter driver (Eq.13), in

which the nonlinear effects of the hardware have also been modelled. Additionally, for comparison, the result of the constant curvature is calculated by using the rest of the measured markers. Even by doing so and using measured and not estimated markers, the mean distances error of the constant curvature method is still larger than our probabilistic method. Since the performance of the model based close-loop control relies on the chosen modelling method, and the constant curvature model presents a larger distance error already at this point, it can be argued that there is no further need to compare the models in close loop experiments.

To summarise, and for the sake of comparison, our data-driven (probabilistic) method (or for that matter, any other similar approach) is a very effective way to learn the input-output behaviour of the catheter steering without requiring a careful analysis and knowledge of the catheter internal design and physical properties, as required with other methods such as PCC, Cosserat rot or minimum-energy. Thus, compared to other high-fidelity modelling approaches, our approach requires less computational resources per time step, less prior knowledge, and is a generic method that could be used for any kind of catheter.

Translational movement. Due to the compliance of the ablation catheter, the catheter main body is uncontrollable in the task level. The global trajectory of the translational movement is highly dependent on the environment constraints and even the gravity. Therefore, in this section we discuss the method in local translational movement, which predicts the local trajectory by using a pre-trained probabilistic model. Fig.6 illustrates the trajectory of the catheter tip with a given translational action δ_l. Due to its compliance property, the trajectory of the catheter tip is normally neither aligned with the translational action of the linear stage nor aligned with the catheter tip. Therefore, in order to estimate the catheter tip movement from the translational actions, the kinematic model Eq.6 needs to be individually trained by the translational actions for the desired tasks, e.g. navigating the catheter in a 3D aorta phantom. After training, the catheter next tip position can be estimated with given current catheter state and translation action: $E[P_{tip_{t+1}}|S_t, \delta_{l_t}]$. Therefore, with given n available insert actions $\delta_{l_i}, i \in (1, n)$, the corresponding available catheter tip P_{tip_i} are estimated, which are considered as the interpolated points of the estimated tip trajectory:

$$\bigcup_{i=0}^{n} (E[P_{tip_i}|\vec{S_t}, \delta_{l_i}]) \tag{14}$$

4.2. Catheter inverse kinematics

For controlling the catheter position in 3D space, the inverse kinematics of the system is required, which calculates the required control actions for given reference positions. In the previous Section 4.1, the forward kinematic strategy

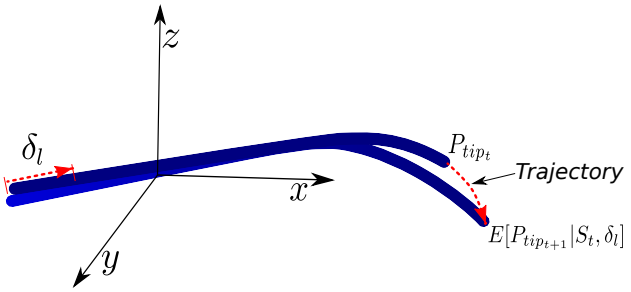

Figure 6: The schematic representation of the catheter tip trajectory with a given translational action δ_l.

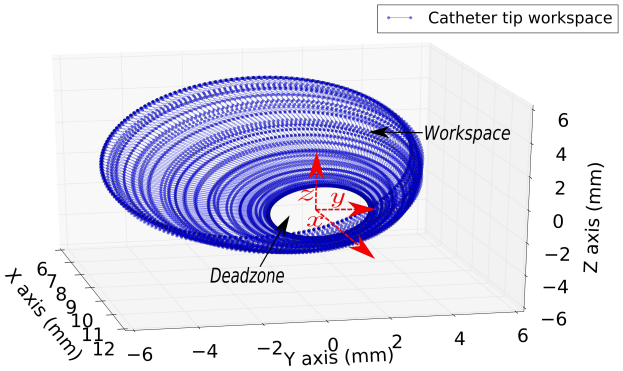

Figure 7: Workspace of the catheter tip with a fixed base position. The blue points represent the reachable positions of the catheter tip by applying pitch and roll actions, that compose a bowl shape surface. The bottom of the bowl surface is empty, which is an uncontrollable space due to the deadzone of the catheter distal section.

is introduced, from which the inverse kinematic is derived. In Fig.4, the result of catheter pitching in one rotation angle is displayed and the trajectory of each marker is plotted. If we rotate the trajectories about an axis, composed by the catheter base point $M6$ and catheter bend point $M5$, the point cloud which consists of the rotated markers represent the workspace of these markers by pitch and roll actions. Therefore, for the sake of drawing the workspace of the catheter tip, the point cloud of M1 in Fig.4 is rotated from 0 to 360 degree about the "base-bend" axis (red dash x axis) and the corresponding workspace is shown in Fig.7. The bowl shape workspace is calculated by rotating the catheter tip in the pitch model Eq.13 around the base axis 360 degrees:

$$T_{W_{tip}} = T_{roll_\theta} T_{pitch_{\delta_{d_i}}} \tag{15}$$

Since the rotation matrix of a point about an arbitrary line is too large for this page, it is simplified to:

$$T_{roll_\theta} = f(P_{tip_i}, M6, M5, \theta) \tag{16}$$

where P_{tip_i} is the catheter tip point clouds with respect to a full pitch-stretch procedure and θ is the roll angle which

is provided by the roll driver. As a result, the workspace of the catheter tip is written as:

$$W_{tip} = \bigcup_{j=0}^{360} \bigcup_{i=1}^{m} f(E[P_{tip_i}|\vec{S_{t_i}}, \delta_{d_i}], M6, M5, \theta_j) \quad (17)$$

Where m are the steps it takes for a full pitch-stretch procedure, which is 74 in our experiments. On this workspace W_{tip}, any selected reference point $P_{tip_{ref}}$ can be positioned by the catheter tip with an appropriate pitch and roll actions. The desired pitch action $\delta_{d_{ref}}$ is estimated by pitch model: $E[\delta_{d_{ref}}|\vec{S_{t_i}}, P_{tip_{ref}}]$ and the roll action is calculated by measured roll angle θ_m and reference angle: $\delta_{\theta_{ref}} = \theta_{ref} - \theta_m$.

Since the reference point normally won't locate on the estimated trajectory, the closest point on the trajectory Trj to the reference point is calculated, which is the actual reference point to estimate the insert action $\delta_{l_{ref}}$:

$$E[\delta_{l_{ref}}|\vec{S_t}, P_{tip_{trj}}] \quad (18)$$

4.3. Catheter position control

In order to automatically steer the catheter tip, a close-loop control framework is developed, which is based on the trained catheter model and the proposed inverse kinematic strategy (see Fig.8). As the figure shows, the control actions $\delta_{l_{ref}}$, $\delta_{d_{ref}}$ and $\delta_{\theta_{ref}}$ are calculated from the inverse kinematic model for given reference positions. In our experiments of trajectory following, the reference inputs are the interpolated points on the designed paths. The calculated three actions are then controlled by the control unit and executed by the linear stage, pitch driver and roll driver of the catheter driver system respectively. The shape of the catheter that is perceived by the near-infrared cameras and the state of the catheter driver are considered as the current state of the system, which is the feedback of the control loop.

Close-loop test in pitch control. The pitch action is controlled in a close-loop by the pitch driver with a visual feedback from the Qualisys cameras. For evaluating the pitch inverse kinematic model $E[\delta_{d_{ref}}|\vec{S_t}, \phi_{ref}]$, the pitch action $\delta_{d_{ref}}$ is estimated with a random selected pitch angle ϕ_{ref} and controlled by a PI controller. The pitch angle is calculated by the measured tip point $M1$, bend point $M5$ and base point $M6$. Fig.9 shows the result of close-loop pitch control to follow desired pitch angles. The pitch model is trained by repeating the full pitch-stretch procedure 30 times and in each procedure 74 observation vectors are captured corresponds to the 74 pitch steps. By using online k-mean update approach (Algorithm 1), 556 mean gaussians are learned for the inverse model. The reference angle is plotted in blue line and actual pitch angle is represented by the red dot line. As the plot shows, the pitch angle of the catheter distal section is controlled to follow the desired angle accurately. Since the hysteresis effect is

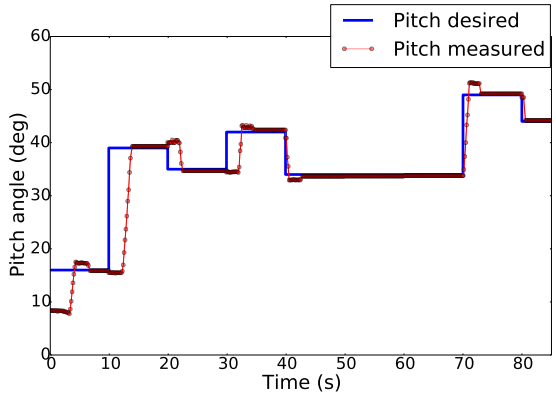

Figure 9: Close loop pitch control of the catheter distal section to follow desired angles.

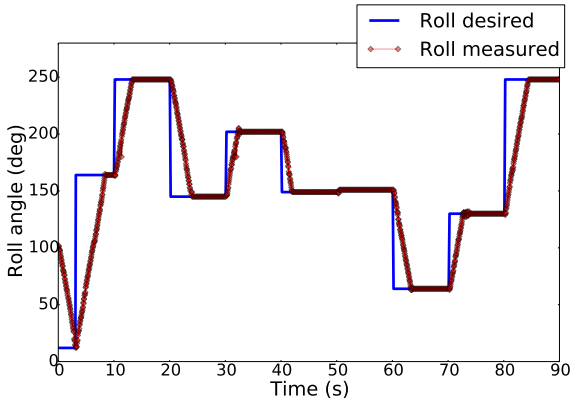

Figure 10: Close loop roll control of the catheter distal section to follow desired angles.

observed in the pitch model and it takes different insert actions to reach the same pitch angel, the control time of the pitch driver (step motor) are different, which can also be observed in the plot that some step responses are much slower than the others.

Close-loop test in roll control. The roll angle of the catheter distal section is defined by the tip point and the base-bend axis, which is initialized to zero at the beginning of a test. During the experiment, the tip point is driven by the roll driver and rotated around the axis. As a result, the rotated angle to the initial state is the roll angle of the distal section, which is controlled by a PI controller in a close-loop and the result is presented in Fig.10. The blue line is the desired roll and the diamond line indicates the actual roll. The control input is selected randomly in a constrained $\theta_{des} \in (0, 360)$ and the results show that the distal roll is regulated to the desired value at a constant speed (maximum speed of the roll driver) with high accuracy.

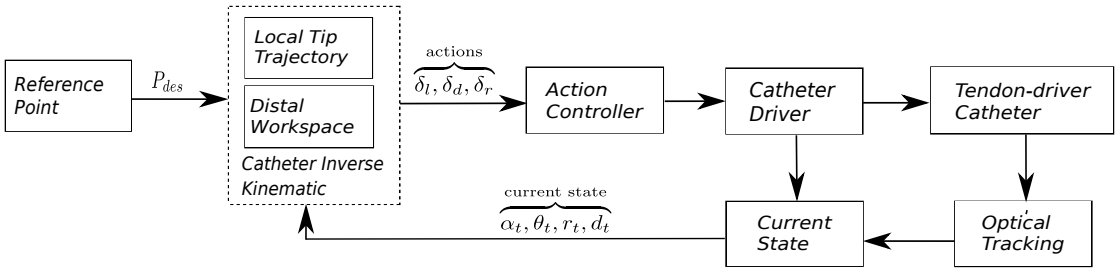

Figure 8: Diagram of a close-loop control for a tendon driven robotic catheter with a visual feedback.

Trajectory following with a robotic catheter driver in a 3D open space. Our goal is to automatically steer the catheter tip to a desired position in 3D space. To evaluate the position control, the square trajectories are used as the desired paths and the reference positions are sampled from the square lines in every 1 mm (see Fig.11). The catheter is driven by the linear stage and inserted along the x axis. The translate, pitch and roll actions are calculated for each desired position and then are steered by the catheter driver in a close-loop until it reaches the goal that its RMSE is smaller than a threshold (2.5 mm). With this approach, the catheter tip is steered to the sampled reference positions consecutively and follows the planned trajectories (red cross line). It can be observed from the figure, the catheter tip is controlled to follow the trajectory closely except the reference positions that locates in the areas of $y_{P_{des}} \in (-14, 14)$ mm. Due to the one-bending direction design and its internal friction and backlash, the EndoSense ablation catheter can not be fully stretched, which derives a dead zone in its workspace. As a result, the reference positions in the dead zones are uncontrollable, which is illustrated in the RMSE result in Fig.12 as well. Since the large errors within the dead zone areas are unavoidable due to the hardware limit of the catheter, it is not included to evaluate the proposed position controller. Therefore the mean RMSE and standard deviation of this test is $e_m \pm std = 1.379 \pm 0.637$ mm.

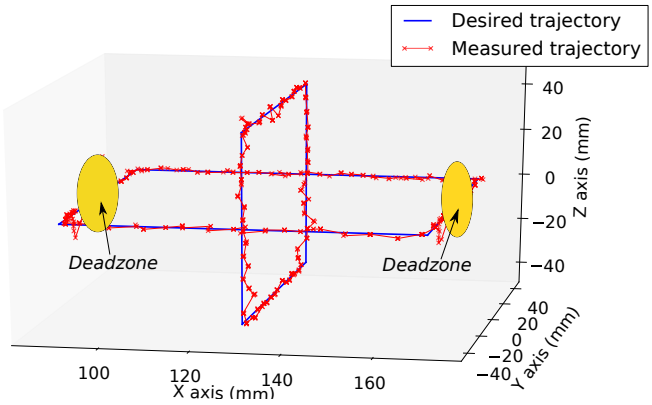

Figure 11: Result of the catheter 3D position control in real 3D open space, the blue squares are the desired trajectories and the red crosses are the catheter tip after steering in each step.

Trajectory following with a simulated catheter in a 3D aorta mesh. In order to further investigate the proposed catheter tip position control in cardiac vascular system, a trajectory following experiment is done by using a catheter simulator which is based on a minimum-energy principle [23].

During testing, the simulated catheter is positioned in a patient-specific vasculature 3D mesh (see Fig.13). The catheter is inserted into the aorta with a constant step of 1 mm and after each insert action, the cross point between the catheter tip workspace to the planned trajectory is calculated as the reference point for catheter distal steering. Based on the trained distal model and the inverse kinematic approach shown in subsection 4.2, the catheter tip is steered to the cross point on the trajectory after each in-

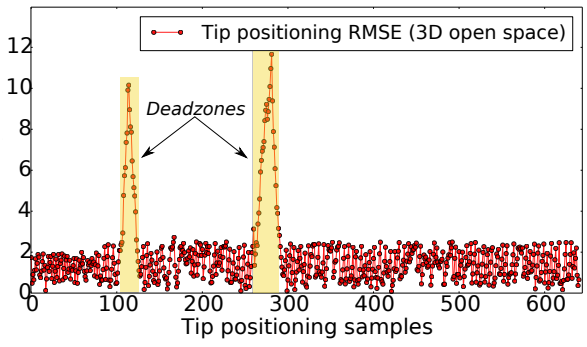

Figure 12: RMSEs of catheter tip positioning in real 3D open space. The red dots represent each RMSE of the catheter tip to the desired position after steering. The yellow areas represent the position errors of reference points which locates in the deadzone of the catheter tip workspace.

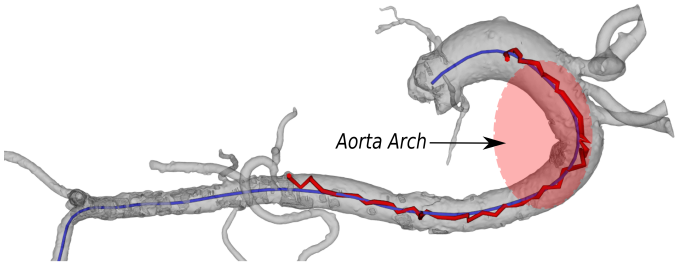

Figure 13: Result of trajectory following in a simulated 3D aorta, the blue line is the desired trajectory and the red line is the catheter tip after steering.

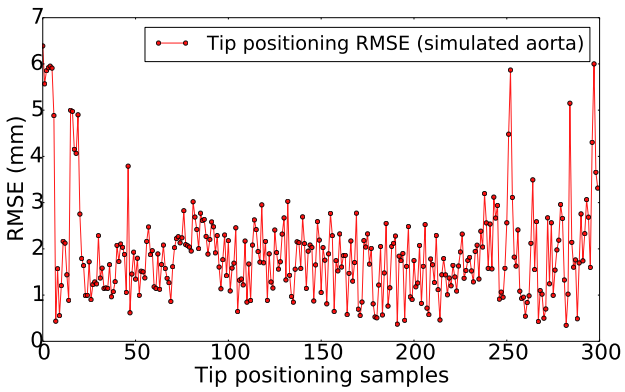

Figure 14: RMSEs of catheter tip positioning by using a FEM based simulated catheter in a patient-specific vasculature 3D mesh. The red dots represent each RMSE of the catheter tip to the desired position after steering.

sert step. As a result, the catheter tip follows the planned trajectory in vascular model by alternatively inserting the catheter and steering the catheter tip to the cross points. Fig.13 shows the result of a catheter trajectory following test. The blue line represents the centerline of the vasculature model, which is calculated from the center points of sectional vessel contour. The red line is the followed trajectory of the catheter tip in the test, which is connected by the steered catheter tip points after insertion every 1 mm. Since aorta arch (see Fig.13) is a challenging section for catheter navigation, the test is started from the middle of vascular model. As can be seen from the Figure, the catheter tip followed the centerline successfully in the test. The tracking error between the catheter tip to the centerline is shown in Fig.14 with a RMSE and standard deviation of $e_m \pm std = 1.909 \pm 1.067mm$.

5. Conclusion

In this paper, a probabilistic model based catheter position control framework is presented, which is able to automatically steer the catheter tip to the desired 3D positions. The learned kinematic model and the proposed position controller are evaluated in a new designed catheter driver system, which firstly applied a "Kellems Grip" to evenly distribute the grip force on the catheter body. The cardiac catheter is tracked by a multiple near-infrared camera system during experiments, which provides an excellent tracking resolution comparing to the EM tracking systems and avoid the self-occlusion problem of the stereo-cameras.

Aimed at precisely controlling the catheter position in a closed form, a dynamic Gaussian mixture model is used which is able to capture the relationship between the catheter states and the control actions in a compact form. The catheter kinematic is approximated to be a combination of a catheter translation model and a catheter distal steering model, addressing external disturbances in translational movement, intrinsic tendon-friction, and backlash in distal steering. The proposed control framework has been validated by 3D trajectory following experiments both in a real 3D open space actuated by a catheter driver system and in a patient-specific vasculature 3D mesh in simulation. In the open space experiment, a tendon-driven ablation catheter could follow a perpendicular squares 3D trajectory with an accuracy of mean RMSE and standard deviation of $e_m \pm std = 1.379 \pm 0.637$ mm and in the vasculature 3D mesh, a simulated catheter could follows the centerline of the aorta with an accuracy of $e_m \pm std = 1.909 \pm 1.067mm$. The results indicate that the proposed control approach is able to accurately navigate the catheter tip to follow a desired 3D trajectory in open space or in a constrained environment. The probabilistic model makes it capable to compensate the basic external disturbances such as gravity and catheter-aorta contact.

For future work, we aim to navigate the robotic catheter inside a real vasculature phantom, in which a more sophisticated interaction model is required for compensating the dynamic effects, e.g. the twist elasticity between the catheter distal to the vessel wall and in the long term, the physiological motions from the heartbeat and blood flow.

Acknowledgment

The authors would like to acknowledge the CASCADE project which was funded by the European Commission's 7th Framework Programme FP7-ICT under grant agreement No. 601021. We would like to thank as well Dr. Yohannes Kassahun and Mr. Abraham Temesgen Tibebu for their assistance in developing the dynamic Gaussian mixture model and Mr. Felix Bernhard for the manufacturing of the catheter driver system.

Author Disclosure Statement

No competing financial interests exist.

References

[1] Webster III RJ, Jones BA. Design and Kinematic Modeling of Constant Curvature Continuum Robots: A Review. *The International Journal of Robotics Research*. 2010;29(13):1661–1683.

[2] Rus D, Tolley MT. Design, fabrication and control of soft robots. *Nature*. 2015;521(7553):467–475.

[3] Renda F, Giorelli M, Calisti M, et al. Dynamic Model of a Multibending Soft Robot Arm Driven by Cables. *IEEE TRANSACTIONS ON ROBOTICS*. 2014;30(5):1109–1122.

[4] Soltani MK, Khanmohammadi S, Ghalichi F, et al. A Soft Robotics Nonlinear Hybrid Position/Force Control for Tendon Driven Catheters. *International Journal of Control, Automation and Systems*. 2017;15(1):54–63.

[5] Kang R, Branson DT, Zheng T, et al. Design, modeling and control of a pneumatically actuated manipulator inspired by biological continuum structures. *Bioinspiration & Biomimetics*. 2013;8(3):036008.

[6] Loschak PM, Brattain LJ, Howe RD. Algorithms for Automatically Pointing Ultrasound Imaging Catheters. *IEEE Transactions on Robotics*. 2017;33(1):81–91.

[7] Back J, Lindenroth L, Rhode K, et al. Model-Free Position control for cardiac ablation catheter steering Using electromagnetic Position Tracking and Tension Feedback. *Frontiers in Robotics and AI*. 2017;4:17.

[8] Tran PT, Smoljkic G, Gruijthuijsen C, et al. Position control of robotic catheters inside the vasculature based on a predictive minimum energy model. In: *In: IEEE International Conference on Robotics and Automation*. 2016; pp. 004687–004693.

[9] Braganza D, Dawson DM, Walker ID, et al. Neural network grasping controller for continuum robots. In: *In Proc. of IEEE Int. Conf. Decision Control*. 2006; pp. 6445–6449.

[10] Giorelli M, Renda F, Calisti M, et al. Neural Network and Jacobian Method for Solving the Inverse Statics of a Cable-Driven Soft Arm With Nonconstant Curvature. *IEEE TRANSACTIONS ON ROBOTICS*. 2015;31(4).

[11] Runge G, Wiese M, Raatz A. FEM-Based Training of Artificial Neural Networks for Modular Soft Robots. In: *In IEEE Int. Conf. on Robotics and Biomimetics*. 2017; pp. 385–392.

[12] Xu W, Chen J, Lau HYK, et al. Data-driven methods towards learning the highly nonlinear inverse kinematics of tendon-driven surgical manipulators. *The International Journal of Medical Robotics and Computer Assisted Surgery*. 2016;13(3).

[13] Lee K, Fu D, Leong M, et al. Nonparametric Online Learning Control for Soft Continuum Robot: An Enabling Technique for Effective Endoscopic Navigation. *Soft Robotics*. 2017;4(4).

[14] Yu B, de Gea Fernández J, Kassahun Y, et al. Learning the Elasticity of a Series-Elastic Actuator for Accurate Torque Control. *Advances in Artificial Intelligence: From Theory to Practice: 30th International Conference on Industrial Engineering and Other Applications of Applied Intelligent Systems, Springer,series LNAI*. 2017;pp. 543–552.

[15] Kellems E. US Patent: US1670543 A Cable Grip, US1670543 A. `https://www.google.com/patents/US1670543A`. 1928. [Online; accessed 08-May-2018].

[16] Jensenius A, Nymoen K, Skogstad S, et al. A Study of the Noise-Level in Two Infrared Marker-Based Motion Capture Systems. In: *In Proceedings of the 9th Sound and Music Computing Conference-Illusions*. 2012; pp. 258–263.

[17] NDI Aurora Electromagnetic Tracking System. `https://www.ndigital.com/medical/products/aurora/`. 2018. [Online; accessed 08-May-2018].

[18] Kato T, Okumura I, Kose H, et al. Tendon-driven continuum robot for neuroendoscopy: validation of extended kinematic mapping for hysteresis operation. *The International Journal for Computer Assisted Radiology and Surgery (IJCARS)*. 2016; pp. 589–602.

[19] Do T, Tjahjowidodo T, Lau M, et al. Dynamic Friction-Based Force Feedback for Tendon-Sheath Mechanism in NOTES System. *International Journal of Computer and Electrical Engineering*. 2014;6:252–258.

[20] Yu B, Tibebu T, Metzen J. Towards catheter pose estimation and data-based catheter steering. In: *In Proceeding of Navigation and Actuation of Flexible Instruments in Medical Application, IEEE /RSJ IROS workshop (NAFIMA)*. 2015; pp. 26–27.

[21] Alderliesten T, Konings M, Niessen W. Modeling friction, intrinsic curvature, and rotation of guide wires for simulation of minimally invasive vascular interventions. *IEEE transactions on biomedical engineering*. 2007;54:29–38.

[22] Hasanzadeh S, Janabi-Sharifi F, Keenan P. Backlash characterization and position control of a robotic catheter manipulator using experimentally-based kinematic model. *Mechatronics*. 2017;44:94–106.

[23] Smoljkic G, Gruijthuijsen C, Vander Sloten J, et al. Towards Intraoperative Use of Surgical Simulators: Evaluation of Catheter Insertion Models. In: *in Proceeding of the 3rd Joint Workshop on New Technologies for Computer/Robot Assisted Surgery (CRAS)*. 2013; pp. 158–160.